Explicit-Solvent Molecular Dynamics Simulations of the β(1→3)- and β(1→6)-Linked Disaccharides β-Laminarabiose and β-Gentiobiose in Water

David Kony,[†] Wolfgang Damm,[‡] Serge Stoll,[§] and Philippe H. Hünenberger*,[†]

Laboratory of Physical Chemistry, ETH Zürich, ETH Hönggerberg, CH-8093 Zürich, Switzerland, Schrödinger, Inc, 120 W 45th Street, New York, New York 10036, and CABE, Department of Inorganic, Analytical and Applied Chemistry, Science II, University of Geneva, 30 Quai E. Ansermet, CH-1211 Geneva 4, Switzerland

Received: October 20, 2003; In Final Form: February 13, 2004

The conformational preferences about the glycosidic linkages present in β-laminarabiose and β-gentiobiose in water are investigated by comparing molecular dynamics (MD) simulations with results from NMR spectroscopy (coupling constants, NOE-derived distances), X-ray crystallography (structures), and molecular mechanics (adiabatic energy maps). The simulations are performed using the OPLS−AA−SEI force field recently developed for hexopyranoses and extended to account for the properties of the linkages present in the two disaccharides. The experimental and theoretical results for β-laminarabiose are very consistent and reveal a clear correlation between the conformation around the dihedral angle ψ and the presence of an interresidue hydrogen bond (from the 4-hydroxyl group of the reducing residue to the ring oxygen of the nonreducing residue). The solvent (water) plays an essential role in determining the preferential orientation about ψ, by dramatically reducing the strength of this intramolecular hydrogen bond. Application of the OPLS−AA−SEI force field to β-gentiobiose requires significant adjustments of the torsional parameters and electrostatic scaling scheme. After optimization of the force field based on ab initio calculations in a vacuum and on the experimental population profile around the dihedral angle ω in water, the OPLS−AA−SEI force field is able to give a realistic representation of the conformational behavior of the β(1→6) linkage on the nanosecond time scale. As expected, the glycosidic dihedral angles in this linkage present an enhanced flexibility compared to the β(1→3) linkage. The results of the two simulations point (in line with previous studies) toward the need of developing a new Karplus-type equation relating hetero-nuclear $^3J_{C,H}$ coupling constants to the glycosidic dihedral angle ϕ. They also suggest that the Karplus-type equation of Stenutz et al. for the homo-nuclear $^3J_{H,H}$ coupling constant is superior to the widely used equation of Haasnoot et al.

Introduction

Disaccharides represent the simplest systems presenting all of the rotational degrees of freedom determining the conformation and flexibility of more complex oligo- and polysaccharides. For this reason, the investigation of the conformational preferences of disaccharides is not only interesting on its own but also an important first step toward the understanding of the conformation and dynamics of polysaccharides. They also represent the simplest test systems for the optimization of any force field ultimately aiming at the simulation of polysaccharide chains. Finally, simulations of disaccharides complement experimental measurements (e.g., from X-ray crystallography and NMR spectroscopy) which have intrinsic limitations due to the important flexibility of these compounds in aqueous solution.[1] Although static structures of mono- and disaccharides are readily obtained from X-ray crystallography, it is always uncertain whether these molecules adopt similar conformations in aqueous solution. On the other hand, NMR spectroscopy provides information of limited resolution in the presence of an equilibrium between multiple conformers in solution. These experimental limitations can be considerably reduced when the experiments are complemented by explicit-solvent molecular dynamic (MD) simulations, because the MD approach provides information over a length and time scale inaccessible to both experimental methods (atomic and femtosecond resolution). When such simulations are in agreement with experiment, they provide detailed insight into the conformational distributions underlying the (time- and space-averaged) experimental results. In practice, combining results from X-ray crystallography, NMR spectroscopy in solution, and MD simulations currently constitutes the most powerful approach for the investigation of the conformational preferences and flexibility of oligosaccharides.

The successful application of simulation methods crucially depends on the description of the interatomic forces and, therefore, on the parametrization of the force field underlying these simulations. The OPLS−AA−SEI force field, an improved version of the OPLS−AA (all atoms) force field for carbohydrates, has been previously described and tested[2,3] against ab initio calculations and experimental data in solution in the context of hexopyranoses. The simulations performed with OPLS−AA−SEI have shown to produce realistic transition frequencies for the hydroxyl groups, and a reasonable population distribution for the hydroxymethyl group in solvated glucose and galactose molecules. The main purpose of this article is to investigate the application of this force field in the context of

* To whom correspondence should be addressed. Phone: +41 1 632 5503. Fax: +41 1 632 1039. E-mail: phil@igc.phys.chem.ethz.ch.
[†] ETH Zürich.
[‡] Schrödinger, Inc.
[§] University of Geneva.

10.1021/jp0371682 CCC: $27.50
Published on Web 04/13/2004

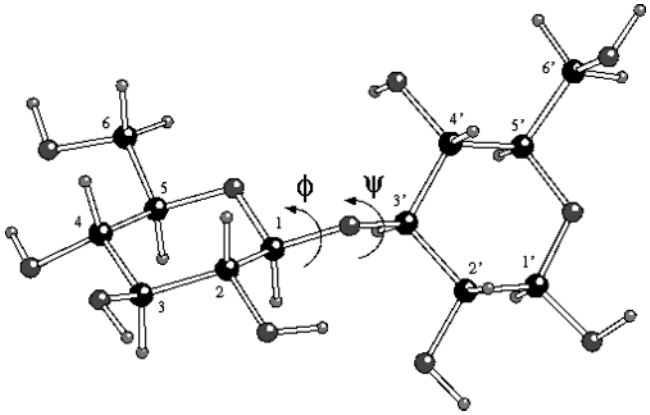

Figure 1. β-Laminarabiose molecule. Carbon atoms are labeled *n* and *n*′ according to the residue they belong to, nonreducing (left) or reducing (right), respectively. Each carbon (Cn) gives its label to the associated hydrogen (HCn) and hydroxyl group (On, Hn). The ring oxygens are labeled O5 and O5′. The glycosidic oxygen is labeled O1.

disaccharide systems, focusing on the description of conformational preferences about the glycosidic linkage.

With the long-term goal of studying schizophyllan,[4] the two disaccharides presenting the linkages characteristic of this polysaccharide have been chosen as test cases, namely, (i) β-laminarabiose, the $\beta(1\rightarrow3)$-linked glucopyranose dimer that is representative of the backbone chain, and (ii) β-gentiobiose, the $\beta(1\rightarrow6)$-linked glucopyranose dimer that constitutes the branching point between backbone and lateral residues. The (1→6) linkage involves a conformational freedom originally arising from the hydroxymethyl group in hexopyranoses, which has been found particularly difficult to reproduce by simulation[3,5,6] and therefore represents a severe test for a force field. In this respect, three of the most promising force fields are CHARMM CSFF,[5] GLYCAM,[6] and OPLS-AA−SEI.[3]

In this paper, explicit-solvent MD simulations of β-laminarabiose and β-gentiobiose in water are reported, which reveal the conformational behavior of two types of glycosidic linkages present in disaccharides that are of great importance in glycobiology.[7] The Karplus-type equations proposed in the literature for the conformational studies of these linkages based on NMR data are also evaluated. The main experimental and theoretical results about the two disaccharides are summarized below.

***β*-Laminarabiose.** The structure of the β-laminarabiose molecule is shown in Figure 1. The relative orientation of the two residues is determined by the dihedral angles ϕ and ψ, defined by the atoms (HC1−C1−O1−C3′) and (C1−O1−C3′-HC3′), respectively, according to established convention.[8] These angles can be determined experimentally by NMR in solution (based on long-range heteronuclear coupling constants across the glycosidic linkage) and by X-ray crystallography in the solid state.

To summarize the conformational preferences of this glycosidic linkage based on experimental data in the solid state, a set of crystallographic structures of D-glucans presenting the $\beta(1\rightarrow3)$ linkage has been taken from the Cambridge Structural Database (CSD).[8] The corresponding glycosidic dihedral angles, as well as selected interresidue oxygen−oxygen distances, are reported in Table 1. Two categories of structures (noted A and B) can be distinguished. The structures of type A have unfunctionalized hydroxyl groups, so that interresidue hydrogen bonds are possible. The structures of type B have substituted hydroxyl groups, which precludes interresidue hydrogen bonds. As expected based on the *exo*-anomeric effect, the dihedral angle ϕ is distributed in a rather narrow range, with a mean value of 42.2°. In contrast, the dihedral angle ψ varies widely between structures of types A and B, with corresponding mean values of −39.7° and 12.7°, respectively.[10] The limits for hydrogen-bonding oxygen−oxygen distances is usually set to 2.7−3.0 Å based on the typical length of hydrogen bonds in alcohols.[11] Crystallographic structures of type A are characterized by an average O4′−O5 distance (Figure 1) of 2.8 Å, which hints toward the presence of an interresidue hydrogen bond. This is in agreement with NMR and IR measurements[12] for laminaran (an oligosacharide with the same glycosidic linkage as laminarabiose) in DMSO, evidencing the presence of one internal hydrogen bond involving a hydroxyl group and a non-hydroxyl oxygen acceptor. For these structures (type A), the hydroxymethyl group of the nonreducing residue is in the gauche−trans (gt) conformation, which causes the O4′ and O6 oxygens (Figure 1) to be in close proximity with an average distance of 3.2 Å, indicating the existence of a weak hydrogen bond between these groups. Finally, large distances are found between the O2′ and O2 atoms (Figure 1) for both structures of types A and B.

TABLE 1: Geometrical Characteristics of a Set of Crystallographic Structures Presenting the $\beta(1\rightarrow3)$-Glycosidic Linkage

structure type	ref[a]	ϕ[b] [deg]	ψ[c] [deg]	O4′−O5 [Å]	O4′−O6 [Å][d]	O2′−O2 [Å]
type A[e]	1	27.6	−37.7	2.78	3.30 (gt)	3.92
	2	31.8	−29.1	2.88	3.14 (gt)	3.57
	3	43.0	−52.2	2.78	3.03 (gt)	4.16
mean A		34.2	−39.7	2.81	3.16 (gt)	3.88
type B[f]	4	49.9	29.0	4.67	6.99 (gg)	3.75
	5	43.2	14.2	3.20	4.75 (gt)	3.61
	6	53.5	10.9	3.10	4.10 (gt)	3.98
	7	42.5	4.4	3.21	4.94 (gg)	3.60
	8	35.0	7.7	3.17	4.70 (gg)	3.65
	9	46.2	10.1	3.11	4.27 (gt)	4.23
mean B		45.9	12.7	3.41	4.96 (−)	3.80

[a] The structures selected are restricted to those involving a limited degree of functionalization and represent a subset of those chosen by French et al. in a previous work.[8] Correspondences between the CSD entry code and the reference number in the table are LAMBIO (1); QUCXER (2); WAGBOV (3); AGPAGP10 (4); DAKKEF (5); FITKAU (6); MHALAM (7); PINLUT (8); and WIMNOV (9). [b] ϕ is estimated as $\phi' - 120°$ where ϕ' is defined by the atoms C2−C1−O1−C3′ (Figure 1). [c] ψ is estimated as $\psi' + 120°$ where ψ' is defined by the atoms C1−O1−C3′−C2′ (Figure 1). [d] The orientation of the hydroxymethyl group in the nonreducing residue is reported between parentheses. The nomenclature refers to two torsional angles: gauche to both O5 and C4 is referred to as gauche−gauche (gg), gauche to O5 and trans to C4 is referred to as gauche−trans (gt), and trans to O5 and gauche to C4 is referred to as trans−gauche (gt). [e] Structures of type A present unfunctionalized exocyclic hydroxyl groups, allowing for interresidue hydrogen bonds. [f] Structures of type B present functionalized exocyclic hydroxyl groups, which precludes interresidue hydrogen bonds.

The $^3J_{C1,HC3'}$ coupling constant for β-laminarabiose octaacetate (that cannot form interresidue hydrogen bonds) measured[13,14] in chloroform is equal to 5.5 Hz (temperature not reported in the article). According to a Karplus relationship (source not cited in the article), this would correspond to a ψ angle of about 0° or 180°, the former value being close to the ψ angles observed for the structures of type B. According to a more recent Karplus relationship for carbohydrates,[15] this would rather correspond to a ψ angle of about 8° or 152°, the former value being in close agreement with the ψ angles observed for most of the structures of type B. The same coupling constant for the disaccharide methyl-β-D-Glc*p*-(1→3)-α-D-Man*p* (that can form interresidue hydrogen bonds) has been measured[16] to be

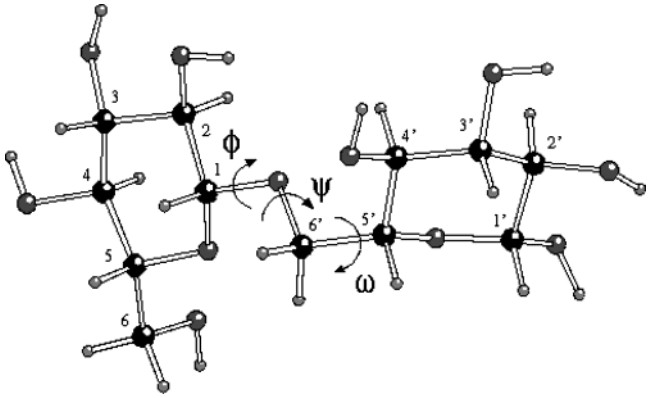

Figure 2. β-Gentiobiose molecule. Carbon atoms are labeled *n* and *n*′ according to the residue they belong to, nonreducing (left) or reducing (right), respectively. Each carbon (Cn) gives its label to the associated hydrogen (HCn) and hydroxyl group (On, Hn). The ring oxygens are labeled O5 and O5′. The glycosidic oxygen is labeled O1.

4.5 Hz in D_2O at 30 °C. The values of the glycosidic dihedral angles for this molecule should be similar to those found in laminarabiose, since the analysis of the crystallographic structures presented in Table 1 suggests that the interaction between the two hydroxyl groups at C2 and C2′ (the later being axial in the above compound and equatorial in laminarabiose) is weak. According to the appropriate Karplus relationship,[15] this coupling constant corresponds to a ψ angle of about 27°, which is again close to the values found for the structures of type B rather than for the structures of type A. The similarity between the ψ values found in water for this disaccharide and those measured in the solid state for compounds which cannot form interresidue hydrogen bonds suggests that the strength of the H4′−O5 hydrogen bond is significantly reduced in water.

Relaxed-residue energy maps for the rotation about the glycosidic linkage in β-laminarabiose, focused around the region of the global minimum, are reproduced in Figure 4, parts b and d, from a study by French et al.[8] based on a combination of molecular-mechanical (MM3 force field) and quantum-mechanical calculations. The maps were computed using dielectric constants of 1.5 (as used for the MM3 parametrization based on gas-phase data) or 7.5 (to mimic a crystallographic environment). The latter value accounts for the weaking of intramolecular hydrogen bonds due to the condensed-phase environment and provides a much better accommodation of the crystallographic structures. The global minimum of the energy map using $\epsilon = 1.5$ is located at $(\phi, \psi) = (40°, -20°)$, in reasonable agreement with crystallographic data for a mixture of α- and β-laminarabiose with $(\phi, \psi) = (27.9°, -37.5°)$,[17] and with the other structures of type A. The structure corresponding to this minimum shows the presence of a H4′−O5 hydrogen bond. The map obtained by reducing the strength of hydrogen bonding[8] using $\epsilon = 7.5$ evidences a considerable shift of the global minimum compared to the map with $\epsilon = 1.5$ and provides, as expected, a much better accommodation of the structures of type B.

***β*-Gentiobiose.** The structure of the β-gentiobiose molecule is shown in Figure 2. The relative orientation of the residues is determined by the dihedral angles ϕ, ψ, and ω, defined by the atoms (HC1−C1−O1−C6′), (C1−O1−C6′−C5′), and (O1−C6′−C5′−HC5′), respectively, according to established convention.[18] These angles can be determined experimentally by NMR in solution (by estimating the proton−proton distances based on NOE intensities, and measuring long-range homo- and hetero-nuclear coupling constant across the glycosidic linkage) and by X-ray crystallography in the solid state.

TABLE 2: Geometrical Characteristics of a Set of Crystallographic Structures Containing the *β*(1→6)-Glycosidic Linkage

structure type	ref[a]	ϕ[b] [deg]	ψ [deg]	ω[c] [deg]	O4′−O2 [Å]	O5′−O2 [Å]
type C[d]	1	45.2	−179.4	167.6 (gg)	3.31	5.70
	2	61.4	−155.1	179.3 (gg)	3.55	5.09
	3	61.7	−156.3	178.4 (gg)	3.54	5.13
mean C		56.1	−163.6	175.1 (gg)	3.47	5.31
type D[e]	4	50.1	−166.8	−45.1 (gt)	4.32	4.49
	5	42.5	−104.1	−53.6 (gt)	4.27	3.82
	6	43.4	160.2	−56.8 (gt)	4.22	4.90
	7	45.3	−175.0	−59.3 (gt)	4.25	4.43
mean D		45.3	−161.5	−53.7 (gt)	4.26	4.41

[a] Correspondence between the CSD entry code and the reference number in the table are: FUNXAN (1), GENTBS (2); GENTBS01 (3); BUFTIF (4); MCRZMA (5); WIMNOV (6); and YEGXEN (7). [b] ϕ is estimated as $\phi' - 120°$ where ϕ' is defined by O5−C1−O1−C6′. [c] ω is estimated as $\omega' + 120°$ where ω' is defined by O6′−C6′−C5′−O5′. [d] Structures of type C are characterized by ω in the gg conformation. [e] Structures of type D are characterized by ω in the gt conformation.

To summarize the conformational preferences of the glycosidic linkage based on experimental data in the solid state, a set of crystallographic structures of D-glucan presenting the β-(1→6) linkage has been taken from the CSD. The corresponding glycosidic dihedral angles, as well as selected interresidue oxygen−oxygen distances, are reported in Table 2. Among the structures, only gg and gt orientations are found for the dihedral angle ω, defining two categories of structures noted C and D, respectively. In contrast, the ϕ and ψ dihedral angles exhibit one predominant orientation of about 50° and −160°, respectively, irrespective of the value of ω. Here also, the *exo*-anomeric effect strongly influences the conformational preferences for the torsional angle ϕ, which is consistent with similar observations for the (1→2)-, (1→3)-, and (1→4)-linked disaccharides,[19] whereas ψ is found to cover a wider range of values compared to ϕ.

The distances between the O4′ and O2 oxygens indicate that favorable interactions can occur when the conformation about ω is gg (type C), whereas the gt orientation (type D) is the preferred conformation for limited favorable interactions between the H2 and O5′ atoms. The ψ dihedral angle can also deviate from its ideal value in order to facilitate this latter interresidue interaction (structure number 5). Similarly, the slight deviation of ψ in structure number 6 is accompanied by a reduction of the distance between the O4′ and O5 oxygens (not shown).

A relaxed-residue energy map of β-gentiobiose has been calculated in the ϕ, ψ, ω space using the MM3 force field[18] with $\epsilon = 4$ (this map is reproduced in Figure 9a−f, right panels). The global energy minimum is located at $(\phi, \psi, \omega) = (42°, 178°, -51°)$ corresponding to a gt conformation around ω. The location of the crystallographic structure of β-gentiobiose[20] on the map, with $(\phi, \psi, \omega) = (63.2°, -156°, -178°)$, corresponds to a relative energy of about 1.6 kcal/mol above the global minimum. However, it has been shown that the difference, which results mostly from ψ (deviating by 24°), is probably associated with crystal packing effects.[18]

The conformation about ω in β-gentiobiose has been extensively studied by NMR.[13,21−23] Early studies estimated the population of the three staggered rotamers from the vicinal $^3J_{HC5',HC6'R/S}$ coupling constants, through the corresponding Karplus equation. More recently, Poppe[21] used simultaneously the information carried by proton−proton and carbon−proton

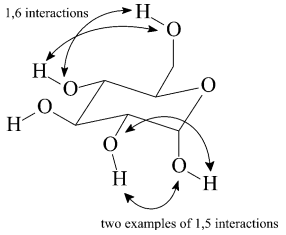

Figure 3. Pairs of atoms defining 1,5 and 1,6 interactions, for which additional (with respect to the OPLS-AA force field) scaling factors are applied in the OPLS−AA−SEI force field, to reduce intramolecular electrostatic interactions. All 1,5 electrostatic interactions within the molecule are scaled by a factor of 1.26, irrespective of the identity of the interacting atoms (only two examples are displayed). The pair of 1,6 interactions involving the hydroxymethyl group and the hydroxyl group at C4 are scaled by a factor 1.22.

vicinal coupling constants together with proton−proton cross-relaxation rates to determine a continuous probability distribution of rotamers. Two dominant conformations characterized by $\omega = 171.1 \pm 6.3°$ (gg) and $\omega = -41.0 \pm 3.4°$ (gt) were found in water, with relative populations of 0.34 and 0.66, respectively. In addition, analysis of cross-peak intensities between the HC1, HC5′, and H4′ protons, and the two prochiral HCR6′ and HCS6′ protons, provides a direct experimental evidence supporting the dominance of the gt conformation in the probability distribution.[10,24] Finally, the absence of the tg conformer is in line with the fact that none of the crystallographic structures reported in Table 2 present this conformation about ω.

The spin−spin coupling constants $^3J_{C6',C2}$ and $^3J_{C6',HC1}$ depend on the ϕ dihedral angle. Their measurement[13] for β-gentiobiose octaacetate in chloroform and interpretation though a Karplus equation (source not cited in the article) has resulted in the established value of 10°. Similarly, the coupling constants $^3J_{C1,HC6'R/S}$ and $^3J_{C1,C5'}$ suggested that ψ is approximately equal to −130°. However, this latter value is highly questionable, since the corresponding article was published at a time where no satisfactory Karplus relationship for hetero-nuclear coupling constants was available.

Computational Methods

The optimization and validation of the OPLS−AA−SEI force field in the context of hexopyranoses was reported previously.[3] One particular feature of this force field is that it requires the scaling of electrostatic interactions for close covalent neighbors. The electrostatic interactions between 1,2 (first) and 1,3 (second) covalent neighbors are completely removed, as usual in classical force fields. The electrostatic interactions between 1,4 (third) neighbors are scaled by a factor of 2, in agreement with the general OPLS-AA approach. However, in the case of hexopyranoses,[3] it was also found necessary to scale all 1,5 interactions by a factor of 1.26 and the 1,6 interactions involving the hydroxymethyl group and the hydroxyl group at C4 by a factor of 1.22 (Figure 3). The 1,5 electrostatic scaling factor was optimized for all types of 1,5 interactions involved in hexopyranoses and hexopyranosides (the latter compounds serving as models for (1→X)-glycosidic linkages), independently of the chemical nature of the interacting atoms. In the case of more complex oligosaccharides, the application of the same 1,5 scaling factor of 1.26 can presumably be extended to the entire molecule, including interresidue interactions. Similarly, the 1,6 scaling factor of 1.22 can also be directly applied to all interactions involving an (unfunctionalized) hydroxymethyl group and its vicinal (unfunctionalized) C4 hydroxyl group. These extensions are sufficient to define the scaling scheme for all oligosaccharides except those involving (1→6)- and possibly also (1→4)-glycosidic linkages. This simple scheme is validated in the present study by comparing MD simulations of the β(1→3)-D-glucan disaccharide β-laminarabiose in water to the experimental information reviewed previously. The definition of the overall scaling scheme for oligosaccharides involving a (1→6) linkage requires additional work. In such a linkage, the hydroxymethyl group is functionalized by a glycosidic bond (Figure 2). The glycosidic oxygen is characterized by a different charge compared to a hydroxymethyl oxygen and cannot act as a hydrogen-bond donor with respect to the hydroxyl group at C4′. As a consequence, the 1,6 scaling factor that (unlike the 1,5 scaling factor) was optimized only for the interaction between unfunctionalized vicinal hydroxymethyl and hydroxyl groups in hexopyranoses is not likely to be adequate for (1→6)-linked disaccharides. Furthermore, in the OPLS−AA−SEI force field, the parameters defining a torsional dihedral potential are determined by the types of the four atoms defining the dihedral angle. The OS−C−C−OS sequence of atoms (in which the two oxygen atoms are "ether oxygens" of type OS) occurring in the case of (1→6)-linked disaccharides has not been encountered previously in hexopyranoses. Thus, no specific parameters are available so far for the OS−C−C−OS dihedral angle potential that drives, together with the C−C−C−OS and the H−C−C−O potentials,[2] the rotation about the C5′−C6′ bond (ω angle).

The two above-mentioned problems are addressed by (i) the introduction and optimization of a different 1,6 scaling parameter for the interaction between a glycosidic oxygen involved in a (1→6) linkage and the hydrogen of the vicinal hydroxyl group and (ii) the introduction and optimization of a new set of parameters for the OS−C−C−OS dihedral potential. Different values for these new parameters are considered and tested in their ability to reproduce gas-phase energies and solution conformations. A 1,6 scaling factor of 1 and the torsional potential parameters corresponding to the free hydroxymethyl group in hexopyranoses (OS−C−C−OH type) were used as initial guess for this optimization procedure. In solution, the population distribution about ω is used as a primary observable to be reproduced, both because the rotation about this bond is very sensitive to the values of the newly-introduced parameters and because data derived from experiments exists for this distribution.[21] In the gas phase, the results of force-field calculations are compared to those of ab initio calculations. The compound 6-O-(1′-methoxy-ethyl)-β-D-Glc*p* (MEG) is a good candidate for such a comparison because it is a simple model that mimics the glycosidic linkage in β(1→6)-D-glucans. This compound is the analogue of β-gentiobiose (Figure 2) with the atoms C2 and C5 replaced by methyl groups. For simplicity, the atom labeling of Figure 2 will be retained for this model compound.

Ab initio calculations were performed on MEG at the HF/6-31G* level of theory. For the initial calibration of the OS−C−C−OS torsional parameters, a rotational profile was determined by varying ω from 0 to 330° by increments of 30°. All other degrees of freedom were optimized, except for the dihedral angles ϕ and ψ and the O1−C1−O5−C5 dihedral angle (Figure 2), which were fixed at 60°, 180°, and 180°, respectively. In addition, the C4′ hydroxyl dihedral angle χ (HC4′−C4′−O4′−H4′) was fixed at −60°, a conformation that favors a counter-clockwise hydrogen-bond network around the glycosidic ring. In this way, the atoms H4′ and O1 cannot form a hydrogen bond during the rotation about ω. The constraints on ϕ and O1−C1−O5−C5 were chosen so that the 1′-methoxy-ethyl sub-

stituent in MEG mimics the configuration of the nonreducing unit in gentiobiose. Those on ψ and χ were chosen so that the energetic profile is dominated by the contribution from the OS−C−C−OS torsional potential. For the refinement of the 1,6 scaling factor, conformations of MEG were generated by varying the χ dihedral angle from 0 to 330° by increments of 30°. In addition to the three dihedral angles mentioned previously, the ω dihedral angle was fixed at 60° for this calculation. This choice leads to the formation and disruption of a H4′−O1 hydrogen bond during the rotation around χ and therefore make the energy profile optimally sensitive to the value of the 1,6 scaling factor. The corresponding rotational energy profiles for the OPLS−AA−SEI force field were determined in a manner analogous to those determined at the ab initio level.

As a next step, MD simulations were performed for β-gentiobiose. The population distributions about ω calculated from the trajectories were compared to experimental values. The scaling factor and torsional parameters were adjusted as long as the agreement between the simulated and experimental population profiles was not met, keeping the force field and ab initio relative energies as close as possible. However, the gas-phase rotational profiles calculated for MEG, which is only a simplified model for the disaccharide, ignore the interaction between the C2 and C4′ hydroxyl groups present in β-gentiobiose. For this reason, agreement with the experimental population distribution could ultimately only be reached by the inclusion of an additional so-called extended scaling factor for the electrostatic interactions between the atoms of the C4′ hydroxyl group and the atoms of the C2 hydroxyl group (see Figure 2).

The procedures followed for the construction of the molecular topology and for performing molecular-mechanics and molecular-dynamics calculations are similar to those described previously for hexopyranoses.[3] For the β-laminarabiose simulations, the system for MD simulation consisted of a single solute molecule surrounded by 1085 TIP3P[25] water molecules. The starting conformation was chosen as that found in the crystal structure of the triple helix of (1→3)-β-D-glucan[26] corresponding to ϕ and ψ angles of 42° and 17°, respectively, and hydroxymethyl groups in the tg and gg configurations for the nonreducing and reducing residues, respectively. For the β-gentiobiose simulations, the system consisted of a single solute molecule surrounded by 1078 TIP3P water model molecules. The crystallographic structure[20] was used as the initial solute conformation, i.e., the configuration of the ω angle and of the hydroxymethyl group of the nonreducing residue are both gg, and the ϕ and ψ dihedral angles are gauche and trans, respectively. This initial conformation was used for all simulations involving different parameters for the 1,6 scaling, OS−C−C−OS torsional potential, and extended scaling parameters.

For all simulations, a time step of 2 fs was chosen to integrate the equations of motion. Bond lengths were constrained by application of the SHAKE procedure[27] with a relative geometric tolerance of 10^{-4}. The cutoff radius for all non−bonded interactions was set to 9 Å based on a pair list updated every five simulation steps. The simulation was performed at 1 atm and 300 K by weak coupling to heat and pressure baths[28] using coupling constants of 0.1 and 0.5 ps, respectively. After a 100 ps equilibration period, the sampling was performed during 10 ns, and configurations were saved every 0.5 ps for analysis.

For β-laminarabiose, averages for the transglycosidic (C1−HC3′ or C3′−HC1) $^3J_{C,H}$ coupling constants (in Hertz) were calculated using the generalized Karplus equation derived by Tvaroska et al.[15]

$$^3J_{C,H} = 5.7\cos^2(\theta) - 0.6\cos(\theta) + 0.5 \quad (1)$$

where θ denotes the ϕ or ψ dihedral angle.

For β-gentiobiose, averages for the homo-nuclear $^3J_{H,H}$ coupling constants (in Hertz) were calculated using the generalized Karplus equations derived by Haasnoot et al.[29]

$$^3J_{HC5',HC6'R/S} = 13.22\cos^2(\omega_H) - 0.99\cos(\omega_H) + \sum\Delta x_i[0.87 - 2.46\cos^2(\xi_i\omega_H + 19.9|\Delta x_i|)] \quad (2)$$

by Imay et al.[30]

$$^3J_{HC5',HC6'R/S} = -1.3556\cos(\omega_H) + 4.9649\cos(2\omega_H) + 1.4627\cos(\omega_H) \times \sum\Delta x_i\cos(\omega_i) - 0.2061[(\tau_1 + \tau_2)/2 - 110] + 6.4068 \quad (3)$$

or by Stenutz et al.[31]

$$^3J_{HC5',HC6'R} = 5.08 + 0.47\cos(\omega_O) - 0.12\cos(2\omega_O) + 0.90\sin(\omega_O) + 4.86\sin(2\omega_O) \quad (4.1)$$

$$^3J_{HC5',HC6'S} = 4.92 - 1.29\cos(\omega_O) + 4.58\cos(2\omega_O) + 0.05\sin(\omega_O) + 0.07\sin(2\omega_O) \quad (4.2)$$

where ω_H denotes the proton−proton dihedral angle (HC5′−C5′−C6′−HC6′R/S) in degrees, ω_O denotes the dihedral angle O5′−C5′−C6′−O1, and τ_1 and τ_2 denote the HC5′−C5′−C6′ and C5′−C6′−HC6′R/S angles in degrees. The index i runs over all substituents on the HC−C−C−HC system, i.e., the atoms O1, O5′, and C4′. These atoms define corresponding dihedral angles ω_i, namely, ω_{O1} (i.e. ω), $\omega_{O5'}$ (O5′−C5′−C6′−HC6′R/S), and $\omega_{C4'}$ (C4′−C5′−C6′−HC6′R/S). Finally, the electronegativity factors (Δx_i) are set to 1.3 (O5′ and O1) and 0.4 (C4′), whereas ξ_i is +1 (syn) or −1 (anti) depending on the relative orientation of the substituent with respect to its vicinal proton.

The hetero-nuclear $^3J_{C,H}$ coupling constants (in Herz) were calculated using the generalized Karplus equations derived by Tvaroska et al.[15,32] namely eq 1 together with

$$^3J_{C4',HC6'S/R} = 0.52 + 5.8\cos^2(\omega_{C4'}) - 1.6\cos(\omega_{C4'}) + 0.28\sin(2\omega_{C4'}) - 0.02\sin(\omega_{C4'}) \quad (6)$$

or an alternative expression derived by Spoormaker et al.[33]

$$^3J_{C4',HC6'S/R} = 3.09 - 0.38\cos(\omega_{C4'} - 5.53) + 2.57\cos(2(\omega_{C4'} - 5.53)) \quad (2)$$

where $\omega_{C4'}$ denotes the proton−carbon dihedral angle C4′−C5′−C6′−HC6′R/S in degrees.

For the analysis of the simulations, the definition used for assessing the presence of a hydrogen bond is based on a geometric criterion. If the distance between the hydrogen of the donor and the oxygen of the acceptor is below 2.5 Å, and the donor−hydrogen−acceptor angle is larger than 135°, the atoms are assumed to participate in a hydrogen bond.

Results and Discussion

***β*-Laminarabiose.** The trajectory of the glycosidic dihedral angles issued from the MD simulation of β-laminarabiose, together with the corresponding MM3-generated energy maps, is displayed in Figure 4. The dihedral angles exhibit a rather low flexibility, with the most populated area lying close the

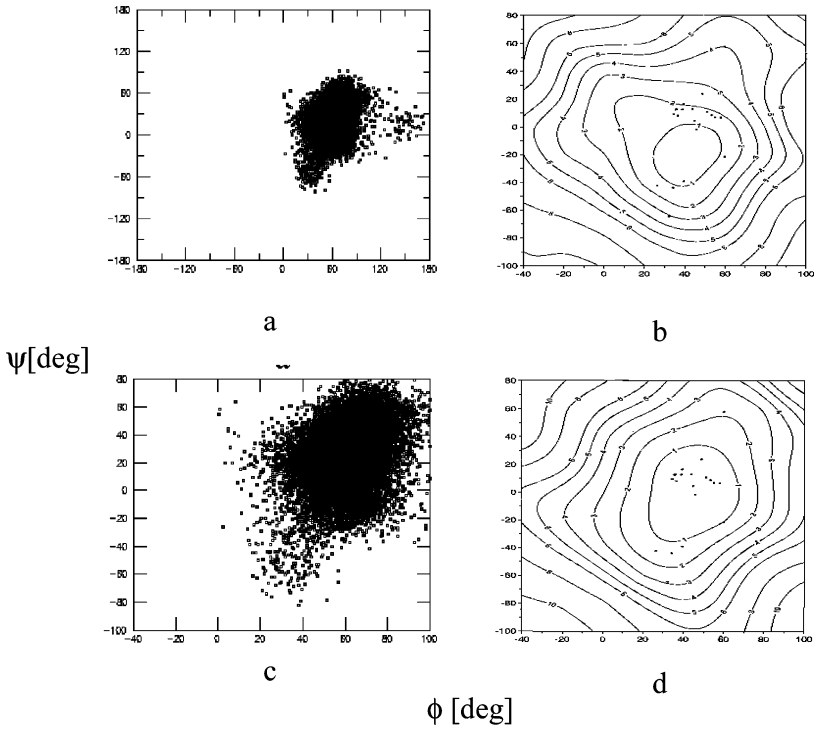

Figure 4. Trajectory of the glycosidic dihedral angles ϕ and ψ during the 10 ns MD simulation of β-laminarabiose, over the complete torsional range (a) and focused around the most populated area (c), together with corresponding hybrid molecular-mechanical/quantum-mechanical energy maps using $\epsilon = 1.5$ (b) and $\epsilon = 7.5$ (d). The two latter maps are reprinted from ref 8, with permission from Elsevier. In (b) and (d), the dots indicate the crystal structures selected by French et al. (a subset of these structures is listed in Table 2).

MM3 lowest-energy region. When comparing parts a and b of Figure 4, it appears that the trajectory actually samples a region with slightly larger ψ values compared to the QM/MM low-energy region encompassing the global minimum for $\epsilon = 1.5$. This shift is, however, considerably reduced when comparing parts c and d of Figure 4, the latter being the QM/MM map calculated with $\epsilon = 7.5$ (reduced strength of intramolecular hydrogen bonds). This result indicates that solvent effects are very important in determining the relative orientation of the two monosaccharide units. It also indicates that, in this case, the mean effect on the linkage conformation of the explicit-solvent model used in the simulation is rather well mimicked by a dielectric medium screening the charge−charge interactions in the MM3 calculations. The same observation can be made when comparing the average of the ϕ and ψ angles during the simulation to the values observed in X-ray structures (Table 1). Agreement for ψ is only met with the X-ray structures of type B, which cannot form interresidue hydrogen bonds. Indeed, interresidue hydrogen bonds, and in particular the H4′−O5 hydrogen bond, are expected to be weak in a polar hydrogen-bonding solvent such as water. In the simulation, this interresidue hydrogen bond, which is the only intramolecular hydrogen bond occurring during 10 ns, is present for only 6% of the configurations.

The time series of the ϕ and ψ dihedral angles, and of specific interresidue hydrogen−oxygen distances, are shown in Figure 5 together with the corresponding probability distributions. The population distribution of the ϕ dihedral angle is rather narrow compared to that of the ψ dihedral angle, as expected from the *exo*-anomeric effect. A short (∼50 ps) transition toward the values corresponding to the MM3 global energy minimum occurs after about 6.3 ns. Simultaneously, the H4′−O5, H6−O4′ and H4′−O6 atom pairs come within close distance (hydrogen-bonding for the first pair). For the two latter atom pairs, the favorable interaction arises because the hydroxymethyl group of the nonreducing residue adopts a gt conformation, as reported for the X-ray structures of type A. The distance distribution for the H4′−O5 pair shows two peaks. The relatively small peak at short distances corresponds to the conformers possessing the H4′−O5 intramolecular hydrogen bond. Although the corresponding population is small, the hydrogen bond itself must be strong because the peak is centered at 1.9 Å. The distance distributions for the H6−O4′ and H4′−O6 pairs also show two peaks. The short-distance peak dominates slightly in the case of the H4′−O6 pair, whereas the opposite is true for the H6−O4′ pair. However, the corresponding distance of 4.1 Å in both cases indicates that the interaction remains weak. Finally, both the H2′−O2 and H2−O2′ distance distributions show only one peak, indicating that the favorable interaction between the two hydroxyl groups involve only one of the two possibles atoms pair. The peak for H2−O2′ is centered at the shortest distance (4.1 Å) so that this interaction remains weak.

The experimental and simulated results characterizing the conformation about the glycosidic linkage in β-laminarabiose are summarized in Table 3. Again, the ϕ dihedral angle is found to vary over a smaller range compared to the ψ dihedral angle, in agreement with the general trend for β-linked disaccharides[19] and as expected from the *exo*-anomeric effect. A very good agreement is found between the simulated and experimental coupling constants for ψ but not for ϕ. The excellent agreement between simulated and NMR data in water for ψ underlines again that the role of the solvent is essential in determining the equilibrium value of ψ and that these effects are accurately captured by the explicit-solvent simulation. Concerning the dihedral angle ϕ, it should be noted that similar discrepancies were previously observed when comparing experimental and simulated results based on three different force fields and considering seven β-linked di- and trisaccharides.[16] As noted by Rundlöf et al., the problem may arise from the interpretation of the transglycosidic $^3J_{C,HC}$ couplings though a unique Karplus-

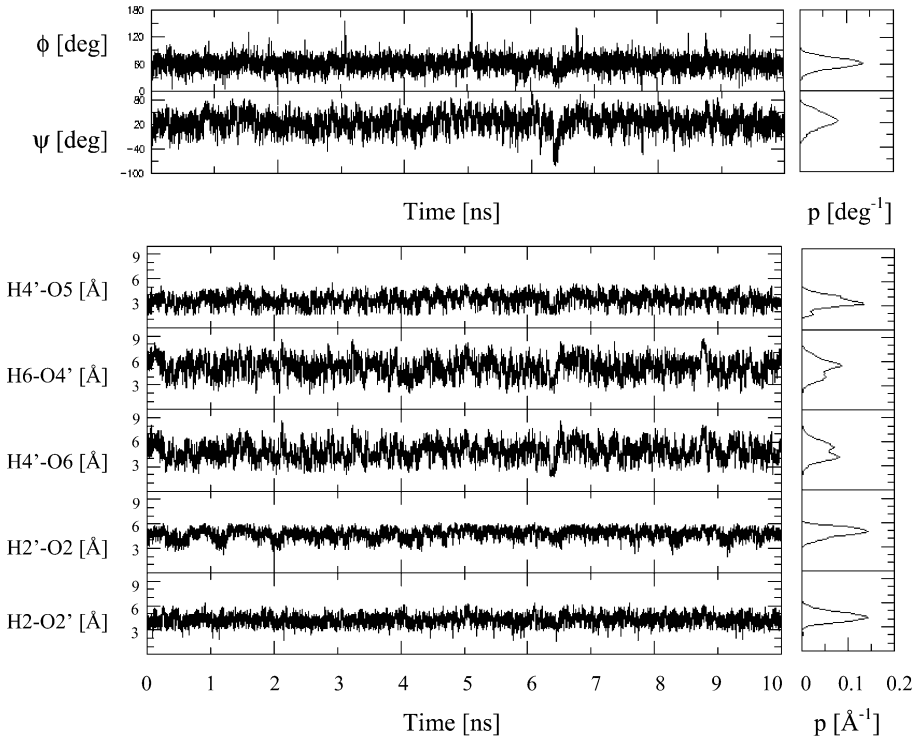

Figure 5. Trajectories of the glycosidic dihedral angles ϕ and ψ, and of selected interresidue hydrogen−oxygen distances, during the 10 ns MD simulation of β-laminarabiose, together with their associated (normalized) probability distributions.

TABLE 3: Experimental and Simulated Results Characterizing the Glycosidic Linkage in β-Laminarabiose

	OPLS−AA−SEI[a]	X-ray		NMR
ϕ [deg]	61.4	34.2[type A]	45.9[type B]	32.1[b]
$^3J_{C3',HC1}$ [Hz]	1.7[b]			4.1[c]
$\Delta\phi$ [deg]	10.2	8.4[d]		
ψ [deg]	25.5	−39.7[type A]	12.7[type B]	26.8[b]
$^3J_{C1,HC3'}$ [Hz]	4.2[b]			4.5[c]
$\Delta\psi$ [deg]	16.9	27.7[d]		

[a] Average property and root-mean-square fluctuation (Δ) calculated over the 10 ns MD simulation. [b] Calculated using the Karplus relationship derived by Tvaroska et al. (eq 1). [c] Measured in D_2O at 30°C for the disaccharide methyl β-D-Glc*p*-(1→3)-α-D-Man*p*;[16] note that, for β-laminarabiose, $^3J_{C1,HC3'} = 5.5$ Hz, in $CDCl_3$,[13] which corresponds to an angle of about 8° (using eq 1). [d] Value averaged over all crystallographic structures (types A and B) reported in Table 1.

type relationship for both ϕ and ψ. Because the substituents at the carbon atoms are different in the two cases, this approach may be questionable. Furthermore, the average value of ϕ during the simulation is only about 15° larger than the corresponding average for the X-ray structures of type B. This suggests that the simulation is realistic in this respect and points toward the need of developing a better Karplus relationship for the specific case of the ϕ dihedral angle.

***β*-Gentiobiose.** The ab initio potential energy profiles for the rotation about the dihedral angles ω and χ (HC4′−C4′−O4′−H4′) of MEG are displayed in Figure 6. As previously found for the rotation of the hydroxymethyl group in hexopyranoses,[3] there is a clear preference for two out of the three rotamers around ω, although the curves also present a flat region with a shallow minimum around 30°. The gg ($\omega \sim 180°$) and gt ($\omega \sim -60°$) rotamers are characterized by nearly identical potential energies, whereas the minimum at 30° is about 3 kcal/mol higher in energy. The rotational profile for the hydroxyl group at C4′ shows only two minima, corresponding to the gauche conformations, which are associated with favorable interactions between the hydroxyl group and its vicinal groups. The g^+ rotamer ($\chi \sim 60°$) is favored over the g^- rotamer ($\chi \sim -60°$) by about 2 kcal/mol.

To evaluate quantitatively the impact of the 1,6 scaling factor within the glycosidic linkage and of the OS−C−C−OS torsional parameters, the ab initio rotational profile about ω in MEG and the corresponding experimental population ratio for β-gentiobiose in solution[21] are compared to the results of OPLS−AA−SEI molecular-mechanics calculations and MD simulations performed: (A) with an initial guess for the OS−C−C−OS potential (OS−C−C−OH parameters for an unfunctionalized hydroxymethyl group) and without scaling factor between the H4′ and O1 atoms; (B) with the same initial guess for the OS−C−C−OS potential and with a scaling factor of 1.22 between the H4′ and O1 atoms (as previously optimized for hexopyranoses); (C) with the introduction of a new set of torsional parameters for the OS−C−C−OS potential and without scaling factor between the H4′ and O1 atoms. The results of these three initial attempts are summarized in Table 4.

In attempt A, the molecular-mechanics potential energy profile for ω in MEG has, in agreement with the ab initio result, the gg and gt conformers as the lowest energy rotamers. However, in contrast to the ab initio calculation, the profile presents a relatively deep minimum at 60° (tg), which is only 2 kcal/mol higher in energy than the global minimum. Finally, there is an incorrect preference for the gg over the gt conformation. This leads to a high population of the tg conformation about ω in the corresponding explicit-solvent MD simulation of β-gentiobiose, in complete disagreement with the experimental ratio. This is a consequence of the interaction between atoms H4′ and O1 (the distance distribution between the H4′ and O1 atoms shows a dominant peak at 1.9 Å, indicating the presence of a hydrogen bond).

The population of the tg rotamer during the course of the MD simulation is considerably reduced in favor of the gg rotamer when comparing attempts A and B, in which the 1,6 scaling factors are set to 1.00 or 1.22, respectively. However,

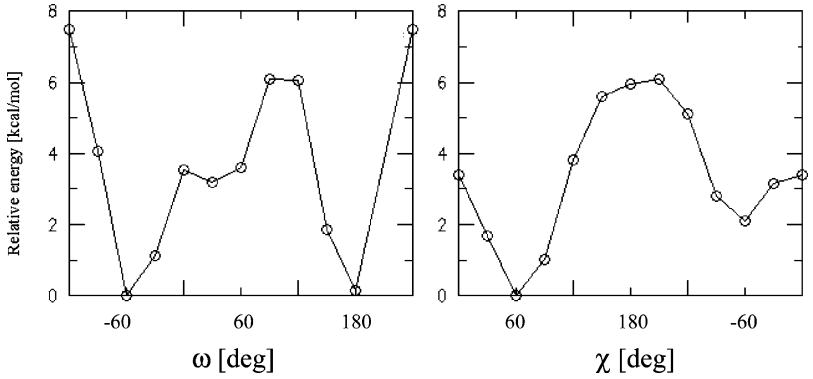

Figure 6. Ab initio rotational potential energy profiles for the rotation about ω (a) and χ (b) in MEG. In both calculations, the dihedral angles ϕ, ψ, and O1−C1−O5−C5 are fixed at 60°, 180°, and 180°, respectively. In addition, in (a), the dihedral angle χ is fixed at −60°, whereas in (b), the dihedral angle ω is fixed at 60°.

TABLE 4: Force Field Attempts for β-Gentiobiose[a]

	parameter sets				MEG			β-gentiobiose				
attempts	1,6 scaling	V1 [kcal/mol]	V2 kcal/mol]	V3 [kcal/mol]	E_{gg} [kcal/mol]	E_{gt} [kcal/mol]	E_{tg} [kcal/mol]	P_{gg} [%]	P_{gt} [%]	P_{tg} [%]	ψ [deg]	ϕ [deg]
ref	1.22	1.593	0.000	0.000	0.10	0.00	3.70	34	66	0	−160	50
A	1.00	1.593	0.000	0.000	0.00	1.03	2.31	4	5	91	−176	60
B	1.22	1.593	0.000	0.000	0.00	0.61	2.67	79	14	7	−171	61
C	1.00	0.702	−0.589	−1.111	0.00	1.03	3.41	40	5	55	−173	62
D	1.15	−1.180	−0.589	−1.589	0.00	0.75	5.10	65	32	3	−172	61

[a] For the four attempts (A, B, C, or D; see text), are reported the selected 1,6 scaling factor (between H4′ and O1) and OS−C−C−OS torsional parameters (dihedral O1−C6′−C5′−O5′; V1, V2 and V3 refer to the coefficients of the cosine terms of multiplicities 1,2 or 3), the molecular-mechanical relative energies of the gg, gt, and tg rotamers about ω in MEG, the average population of the corresponding rotamers in β-gentiobiose obtained from a 10 ns explicit-solvent simulation, and the corresponding average values of ϕ and ψ. The first line (ref) indicates the parameter set used in the case of hexopyranoses,[3] the ab initio relative energies of the conformers (see Figure 6), the relative conformer populations from experiment,[21] and the values of ϕ and ψ averaged over all the X-ray crystallographic structures of Table 2.

as a consequence, the population of the gg rotamer is too large compared to experimental data. As seen from the analysis of crystallographic structures (Table 2), a favorable interaction between the C2 hydroxyl group of the nonreducing residue and the C4′ hydroxyl group of the reducing residue may be partly responsible for the too high stability of the gg configuration during the simulation, the proximity between these two groups being lost when ω is in the gt configuration. In addition, the lifetime of the gg rotamer, i.e., the time between two transitions, is over 4 ns (data not shown), which is very long compared to the corresponding lifetime for rotamers of the hydroxymethyl group in hexopyranoses (about one nanosecond).[34]

In attempt C, the OS−C−C−OS torsional parameters have been chosen in order to adjust the ab initio and molecular-mechanics potential energies in the region $\omega = 60°$ (tg conformer), while no 1,6 scaling is applied. Compared with the original OPLS−AA−SEI profile (attempts A and B), the depth of the potential well corresponding to the tg conformer is reduced, which improves the agreement with the ab initio calculations. The heights of the potential energy barriers at −120° and 120° are also slightly reduced (data not shown). Although the associated MD simulation presents an increased number of transitions (data not shown), the population ratio is still inconsistent with experimental data.

The above MD simulations indicate that both the 1,6 scaling factor and the OS−C−C−OS torsional parameters play a key role in determining the distribution of the rotamers about ω in β-gentiobiose. Clearly, the electrostatic interactions between the atoms H4′ and O1 must be reduced to prevent the dominance of the tg conformer. However, the value of 1.22 for the corresponding 1,6 scaling factor developed for hexopyranoses appears to be inadequate for the (1→6) linkage. To estimate an appropriate value for this case, the ab initio potential energy

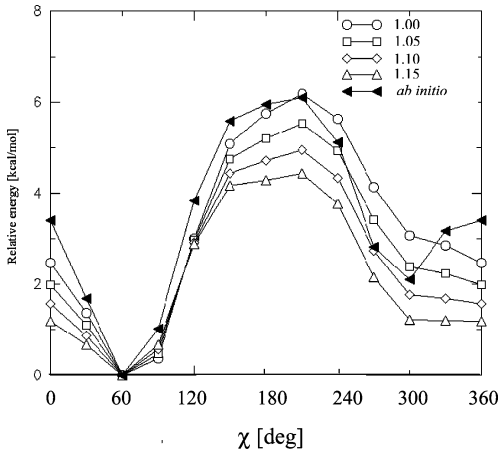

Figure 7. Ab initio and molecular-mechanical potential energy profiles for the rotation around χ (HC4′−C4′−O4′−H4′) in MEG. The different molecular-mechanical curves correspond to different values of the 1,6 electrostatic scaling factor between atoms H4′ and O1. The dihedral angles ϕ, ψ, ω, and O1−C1−O5−C5 are fixed at 60°, 180°, 60°, and 180°, respectively.

profile of MEG for the rotation about the hydroxyl group at C4 (Figure 6) is compared in Figure 7 to the corresponding molecular-mechanics profile for different values of the scaling factor. A value comprised between 1.05 and 1.10 allows the OPLS−AA−SEI force field to reproduce the ab initio energy difference between the conformers corresponding to $\chi = 60°$ (hydrogen bond H4′−O1) and $\chi = -60°$ (hydrogen bond H4′−O3′). However, it should be noted that the conformer with $\chi = -60°$ is not represented by the force field as a stable minimum, in contrast to the ab initio calculations. The relative energy calculated for this conformer is underestimated by the force

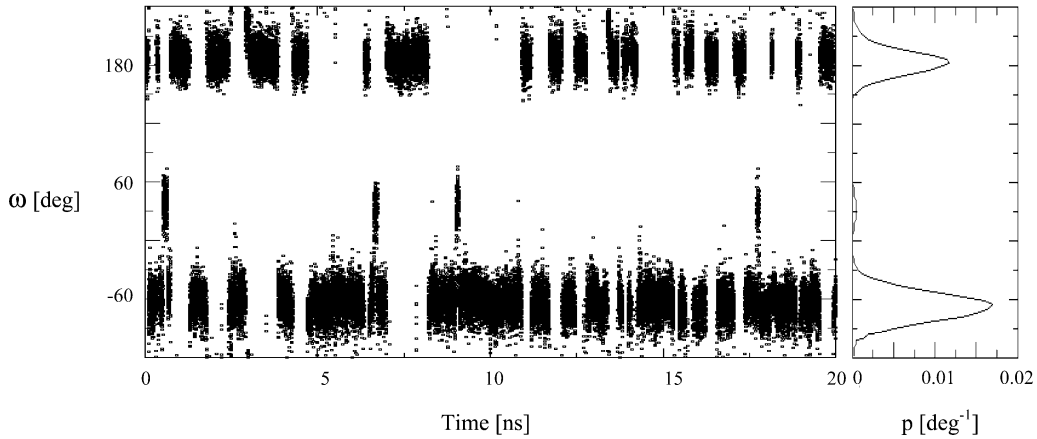

Figure 8. Trajectory of the dihedral angle ω during the 20 ns simulation of β-gentiobiose, together with its associated (normalized) probability distribution, as obtained with the final (optimized) set of OPLS−AA−SEI force field parameters. The 1,6 and extended scaling factors are set to 1.10, and the torsional parameters used for the OS−C−C−OS dihedral angle are identical to those used in attempt D (Table 4).

field compared to the ab initio calculations when using the value of 1.15 for the scaling factor. However, this choice presents the advantage of representing it as a shallow minimum.

Based on the above considerations, a new force field attempt was undertaken, associating a 1,6 scaling factor of 1.15 with a reoptimized torsional parameter set. The results of this new attempt D are summarized in Table 4. The relative energy of the tg conformation in the molecular-mechanical rotational profile increases to about 5 kcal/mol, whereas the barrier at −120° decreases to 3.5 kcal/mol (data not shown). As expected, this increases the number of transition between the gg and gt rotamers during the simulation (data not shown) and reduces the population of the tg rotamer. However, the MD simulation still fails to reproduce the experimental gg/gt population ratio.

Inspection of the gas-phase rotational profiles for attempts A−D suggests a reason for this failure. In a vacuum, the OPLS−AA−SEI force field systematically favors the gg rotamer over the gt rotamer by about 1 kcal/mol, in disagreement with the ab initio calculation where the two conformers are equally stable. The gg/gt gas-phase energy gap could be modulated by the introduction of an additional term with multiplicity one and phase shift −120° into the OS−C−C−OS torsional parameter set. Although rather artificial, this method permits to probe whether the gg/gt population ratio in the MD trajectory for β-gentiobiose results from a difference in the gg and gt relative energies as calculated in a vacuum for MEG. This investigation showed that even inverting the gg/gt relative energies in favor of the gt rotamer for MEG failed to significantly decrease the gg rotamer population in the β-gentiobiose simulation in solution (data not shown). Thus, it appears that the gg/gt population ratio is sensitive to interactions that are not present in the MEG molecule.

As suggested by the X-ray structures of type C (Table 2), the enhanced stability of the gg configuration in β-gentiobiose by the force field may be related to an overestimation of the interaction between the C4′ and C2 hydroxyl groups compared to the interaction between the C2 hydroxyl group and the O5′ ring oxygen (the latter favoring the gt configuration). This problem may be remedied by the introduction of a so-called extended scaling factor applied to electrostatic interactions involving atoms of the two former groups. This approach was tested in a series of new force field attempts with different values for this extended scaling factor and the same OS−C−C−OS torsional parameters as in attempts D (data not shown). It turned out that the extended scaling indeed plays a key role in modulating the gg/gt population ratio and can be used to enforce the domination of the gt rotamer during the course of a MD simulation. An optimized value of 1.10 (for both the extended scaling factor and the 1,6 scaling factor) considerably reduced the number of visits of the gg rotamer, caused a dramatic increase in the number of transitions, and allowed the experimental gg/gt population ratio to be accurately reproduced by the MD simulation. The corresponding trajectory of the dihedral angle ω (together with the associated normalized probability distribution) is displayed for a 20 ns simulation in Figure 8. The resulting population ratio is gg:gt:tg = 36:62:2, in excellent agreement with the experimental ratio of 34:66:0. This last set of parameters defines the final OPLS−AA−SEI force field extended for the application to (1→6)-glycosidic linkages. The MD trajectories of the (ϕ,ψ) glycosidic dihedral angles for β-gentiobiose are presented in Figure 9 for different values of ω together with the corresponding MM3 gas-phase energy map. The corresponding trajectories of the dihedral angles ϕ and ω, as well as ψ and ω, are displayed in Figure 10. The MD trajectories reproduce the MM3 energy landscape quite well. In agreement with the gas-phase calculations, the disaccharide adopts preferentially an extended configuration (with the two ring in a trans orientation relative to ψ) but with a high degree of flexibility (values ranging from −60° to +60°). Although the conformational preference for ϕ during the simulation remains within the MM3-delimited domain, the trans configuration of ϕ presents a nonnegligible population indicating a larger flexibility around the dihedral angle ϕ in β-gentiobiose compared to β-laminarabiose (where the trans configuration of ϕ was barely visited). It is interesting to note that the trans conformation about ϕ principally occurs during the simulation when ω is in the gg configuration (Figure 10). The only significant differences between the MD trajectory and the MM3 calculations are found with $\omega \sim -120°$. This region is visited more often during the course of the simulation than expected based on the MM3 energy map. However, the conformer population corresponding to this region remains limited (less than 5% over the 20 ns simulation), possibly indicating unstable conformers sampled during a transition of ω between the gg and gt configurations. During the transitions between the staggered rotamers about the dihedral angles ω, ϕ and ψ tend to remain close to their ideal values of 60° and 180°, respectively. Nevertheless, the ψ dihedral angle can sometimes adopt values between −90 and −60° when ω undergoes a transition between the gg and gt configurations. This type of conformation, found experimentally in the case of X-ray structure number 5 in Table 2, is due to the appearance of a

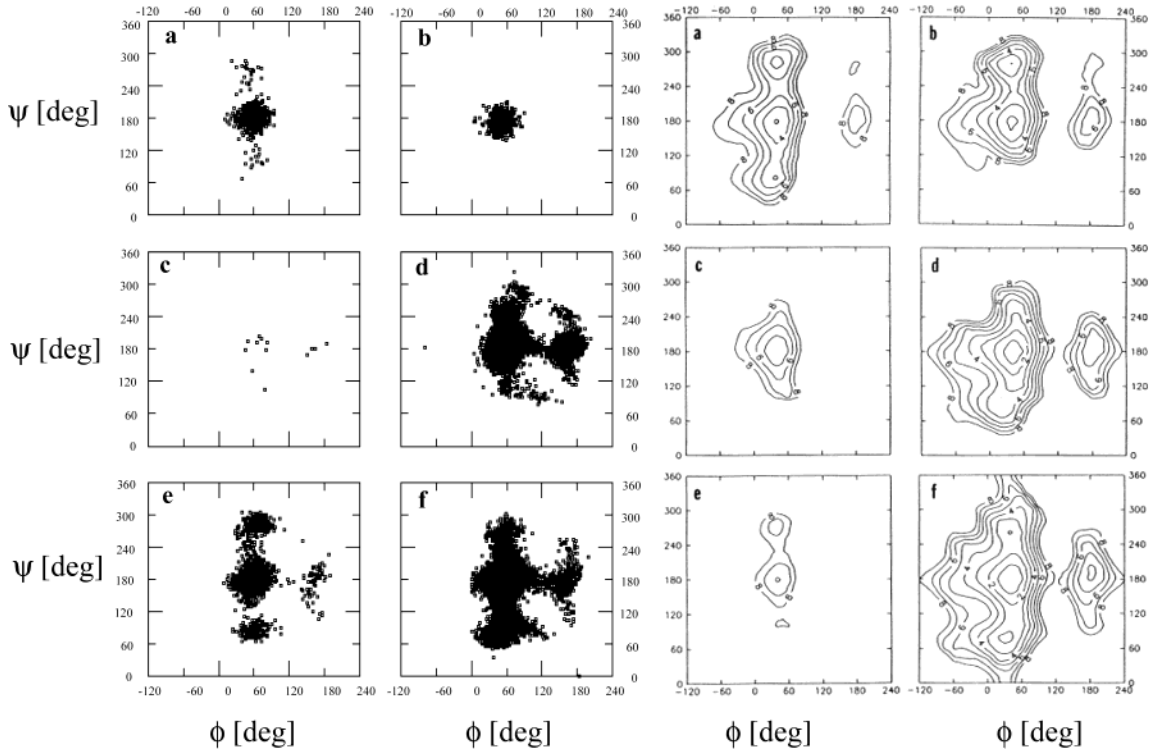

Figure 9. Trajectory of the glycosidic dihedral angles ϕ and ψ during the 20 ns simulation of β-gentiobiose with the final set of OPLS−AA−SEI parameters. The trajectories during the MD simulation (left) are presented together with the corresponding MM3-generated maps (right; with $\epsilon = 4$) for ω values in a range of $\pm 30°$ around (a) $\omega = 0°$, (b) $\omega = 60°$, (c) $\omega = 120°$, (d) $\omega = 180°$, (e) $\omega = -120°$, and (f) $\omega = -60°$ (MM3-generated maps reprinted from ref 18 with permission from Wiley).

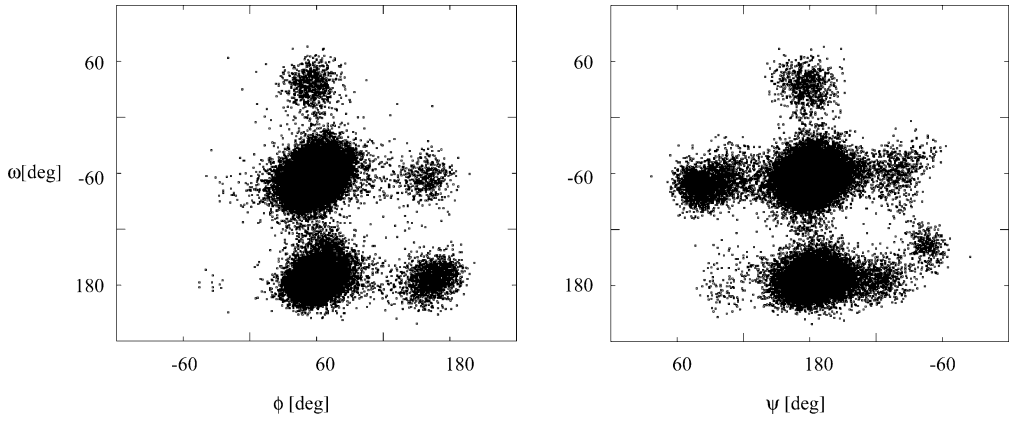

Figure 10. Trajectory of the glycosidic dihedral angles ϕ and ω (a) or ψ and ω (b) during the 20 ns MD simulation of β-gentiobiose with the final set of OPLS−AA−SEI parameters.

favorable interresidue interaction between the H2 and O5′ atoms, although a corresponding interresidue hydrogen bond was never found during the entire MD trajectory.

The conformer populations and mean dihedral-angle values for β-gentiobiose obtained from NMR spectroscopy, X-ray crystallography, MM3 calculations, and MD simulations are compared in Table 5. The different values for the ϕ and ψ dihedral angles are in reasonable agreement. The difference between the mean angles for ψ obtained from the simulation and from the X-ray crystallographic structures (about 20°) is probably due to packing effects in the crystal.[18] As noted previously, the simulated and experimental population ratio about ω agree extremely well. However, divergences are found between the different techniques with respect to the mean ω values corresponding to the gg and gt rotamers. The simulated values differ from the corresponding NMR (X-ray crystallography) values by about 20° (10°) for both the gg and gt configurations. A comparison between experimental observables (hetero- and homo-nuclear coupling constants; NOE-derived distances), values estimated from molecular-mechanics calculations, and the corresponding values calculated from the present MD simulations is presented in Table 6. The experimental rotamer distribution about ω and the corresponding mean angle values determined by Poppe et al. relied on the hetero- and homo-nuclear coupling constants ($^3J_{C4',HC6'R}$, $^3J_{C4',HC6'S}$, $^3J_{HC5'HC6'R}$, and $^3J_{HC5'HC6'S}$), and NOE-derived distances (HC5′−HC6′R, HC5′−HC6′S, HC4′−HC6′R, and HC4′−HC6′S) that are reported in this table. The author used the Karplus-type equation parametrized by Spoormaker et al.[33] for the hetero-nuclear coupling constants and the Karplus-type equation parametrized by Haasnoot et al.[29] for the homo-nuclear coupling constants. When using these equations, the coupling constant calculated from the MD simulation and the corresponding experimental values present significant deviations (1.2−2.9 Hz). Considering

TABLE 5: Conformer Populations and Mean Dihedral-Angle Values for β-Gentiobiose, Evaluated by NMR Spectroscopy, X-ray Crystallography, MM3 Calculations, and MD Simulations

	ω						
	relative population [%]			mean angle [deg]			
	gt	gg	tg	gt	gg	ψ [deg]	ϕ [deg]
NMR[a]	66 ± 6	34 ± 6	0.00	−41.0 ± 3.4	171.9 ± 6.3		
X-ray[b]	4/7	3/7	0/7	−54	175	−162.4	50
MM3				−51.1[c]	175.6[d]/180.0[e]	178.4[c]/179.2[d]/−156.1[e]	42.5[c]/42.6[d]/56.4[e]
OPLS−AA−SEI	62	36	2	−63.5	−171.8	−177 (90%[f])	59.2 (95%[f])
						88 (6.5%[f])	161.3 (5%[f])
						−95 (3.5%[f])	

[a] For ω, see ref 21. For ϕ and ψ, data from the literature are too ambiguous to serve for the comparison. [b] Dihedral angle values are averaged over the seven X-ray structures reported in Table 2. [c] Global minimum of the MM3 map[18] ($\epsilon = 4$). [d] Second minimum of the MM3 map[18] ($\epsilon = 4$). [e] Minimum found when the MM3 calculations are performed for a β-gentiobiose mini-crystal.[18] [f] Population ratio.

TABLE 6: Comparison between Theoretical and Experimental Values for Coupling Constants and NOE-Derived Distances Across the β(1→6) Linkage

	NMR([a])	MM3	MD
$^3J_{C4',HC6'R}$ [Hz]	1.0(0.5)[b]		2.2[c]/1.7[d]
$^3J_{C4',HC6'S}$ [Hz]	3.0(0.5)[b]		3.0[c]/3.5[d]
$^3J_{HC5'HC6'R}$ [Hz]	6.0(0.1)[b]	7.4[e,f]	7.9[f]/7.2[g]/6.5[h]
$^3J_{HC5'HC6'S}$ [Hz]	2.0(0.1)[b]	2.7[e,f]	4.0[f]/3.7[g]/2.9[h]
$10^3 \times$ HC5′−HC6′R [Å^{-6}]	2.64(0.51)[b]		2.44[i]
$10^3 \times$ HC5′−HC6′S [Å^{-6}]	4.16(1.00)[b]		5.15[i]
$10^3 \times$ HC4′−HC6′R [Å^{-6}]	3.12(0.67)[b]		3.14[i]
$10^3 \times$ HC4′−HC6′S [Å^{-6}]	1.68(0.47)[b]		1.03[i]
$^3J_{C6',HC1}$ [Hz]	3.8[j]/3.4[k]	3.2[e,l]	2.1[l]
$^3J_{C1,HC6'R}$ [Hz]	4.0[j]/3.9[k]	1.8[e,l]	2.4[l]
$^3J_{C1,HC6'S}$ [Hz]	2.0[j]/2.6[k]	2.0[e,l]	2.0[l]

[a] Error on the experimental value. [b] From ref 21, based on β-gentiobiose dissolved in $D_2O/(CD_3)_2CO$ (4:1,v/v), at 301 K for the NOE measurements, whereas the temperature for the coupling constant measurements is not reported. [c] $^3J_{C,H}$ determined using the Karplus-type equation derived by Spoormaker et al.[33] [d] $^3J_{C,H}$ determined using the Karplus-type equation derived by Tvaroska et al.[15] [e] From ref 18, based on the Boltzmann-weighted average of values calculated for the 10 local minima present in the MM3 map. [f] $^3J_{H,H}$ determined using the Karplus-type equation derived by Haasnoot et al.[29] [g] $^3J_{H,H}$ determined using the Karplus-type equation derived by Imai et al.[30] [h] $^3J_{H,H}$ determined using the Karplus-type equation derived by Stenutz et al.[31] [i] Based on r^{-6} averaging of the instantaneous proton−proton distance during the simulation. [j] ^3J for β-gentiobiose octa-O-acetate in $CDCL_3$, temperature not reported in the article.[13] [k] ^3J for β-gentiobiose octa-O-acetate in $CDCL_3$, temperature not reported in the article.[14] [l] $^3J_{C,H}$ determined using the Karplus-type equation derived by Tvaroska et al.[15]

that the simulation correctly reproduces the experimental gg/gt population ratio and NOE derived distances, this result could arise from the use of an inaccurate Karplus-type equation to calculate the coupling constant. Indeed, new Karplus-type equations have recently been developed to assist in the structural interpretation of coupling constants in carbohydrates. These more recent equations are generally parametrized using a combination of experimental and theoretical results, leading to a significantly improved level of accuracy. In 1995, Tvaroska et al.[32] used theoretical methods to develop parameters for evaluating hetero-nuclear carbon−proton ^3J coupling constants, specially designed for conformational studies of the hydroxymethyl group in carbohydrates. Imai et al.[30] in 1990 and later Stenutz et al.[31] in 2002 also developed parameters for homonuclear proton−proton ^3J coupling constants. These three more recent Karplus-type equations have also been used to calculate coupling constants from the MD simulation (Table 6). As expected, the deviations between simulation and experiment are significantly reduced, and reasonable agreement with the experimental data is finally achieved when using the Karplus-type equations of Stenutz et al. for the homo-nuclear coupling constant (eqs 4.1 and 4.2) and the one of Tvaroska et al. for the hetero-nuclear coupling constant (eq 6). This suggests that the population profile of Poppe may need to be rederived using these newer Karplus-type equations. However, in our opinion, the improvement that could be achieved by using these new Karplus-type equations will probably be offset by the intrinsic uncertainties inherent to Poppe's method. On one hand, the method applied by Poppe has the advantage of accounting simultaneously for several NMR parameters and for experimental errors, and of generating a continuous population distribution for ω without a prior knowledge of rotameric states unlike other standard methods based on discrete conformational states.[21] On the other hand, this method leads to a set of equally acceptable solutions for the population profile, which present a quite large dispersion. Taking an average of these multiple solutions (as done by Poppe) is then questionable.

The $^3J_{C6',H1}$ coupling constant is a conformational probe for the dihedral angle ϕ. In contrast to the value calculated for the minima of the MM3 energy map, the coupling constant evaluated from the MD simulation is underestimated. However, this result is consistent with similar observations made in the case of the β-laminarabiose as well as other di- and trisaccharides.[16] This systematic discrepancy suggests that the parameters developed by Tvaroska et al. in 1989 for this coupling constant are not adequate for the derivation of the dihedral angle ϕ. Finally, the values of the $^3J_{C1,HC6'S}$ and $^3J_{C1,HC6'R}$ coupling constants calculated from the simulation are quite similar, which reflects the fact that ψ is close to 180° on average. In contrast, the two experimental coupling constants differ nonnegligibly, which indicates a deviation from the ideal trans conformation. However, in contrast to the MM3 prediction, the ranking of the two coupling constants is still correctly reproduced in the values calculated from the MD simulation.

Conclusion

The extension and application of the OPLS−AA−SEI force field to the β(1→3)- and β(1→6)-linked disaccharides β-laminarabiose and β-gentiobiose has been investigated. This extension requires the optimization of a new electrostatic scaling scheme and of a new type of dihedral-angle potential. The results of the MD simulations based on the optimized force field are found to agree well with the available experimental data on the two disaccharides.

In the case of β-laminarabiose, the extension of the force field merely requires the systematic application of the 1,5 and 1,6 (hydroxymethyl groups with vicinal hydroxyl groups) scaling factors developed for hexopyranoses to all corresponding interactions within the entire molecule. The simulation, together

with experimental data, reveals the importance of the interresidue OH4′−O5 hydrogen bond in determining the conformational equilibrium about the ψ dihedral angle and shows that, by attenuating the strength of interresidue hydrogen-bonds compared to the gas-phase, the solvent (water) plays a significant role in determining the relative orientation of the two monosaccharide units.

In the case of β-gentiobiose, the extension of the force field requires some more changes. These included (i) the development of a specific torsional type for the OS−C−C−OS atom sequence, (ii) the application of the 1,5 and 1,6 (unfunctionalized hydroxymethyl groups with vicinal hydroxyl groups) scaling factors developed for hexopyranoses to all corresponding interactions within the entire molecule, (iii) the application of a new 1,6 scaling factor (glycosidic oxygen in (1→6) linkage with vicinal hydroxyl group), and (iv) the application of a new extended scaling factor (hydroxyl groups at C2 and C4′ vicinal to a (1→6) linkage). The extended structure is the preferred conformation of β-gentiobiose, with the ring oriented *trans* relative to ψ. As expected, and in agreement with the experimental data,[35] the simulation shows a larger dihedral-angle flexibility about the β(1→6) linkage compared to the β(1→3) linkage. The glycosidic dihedral angle ψ is characterized by a high degree of flexibility, whereas ϕ presents the most restricted motion, with an average value dictated by the *exo*-anomeric effect. Nevertheless, the trans configuration about ϕ, which occurs especially when ω is in the gg configuration, is also encountered more often in gentiobiose compared to laminarabiose. The experimental population ratio about the glycosidic dihedral angle ω is well reproduced by the MD simulations on the nanosecond time scale.

The results also suggest, in line with previous observations,[16] that the Karplus-type equation proposed by Tvaroska et al. for the transglycosidic $^3J_{C,H}$ coupling constants is not very accurate for the determination of the ϕ dihedral angle. In addition, in the case of the β(1→6) linkage, the results point toward a better accuracy of the Karplus-type equations developed by Stenutz et al. for homo-nuclear coupling constants and by Tvaroska et al. for hetero-nuclear coupling constants compared to previously developed equations.

After the present optimization, the OPLS−AA−SEI force-field parameters should provide a good starting point for extension to other types of glycosidic linkages involved in hexopyranose-based polysaccharides. Nevertheless, careful validation (and possibly further refinement) may be required before this goal is reached. In particular, special attention will be paid to α linkages (not considered in the present study) and to the (1→4) linkage (because the C4 hydroxyl group involves a 1,6 scaling factor currently only optimized for hexopyranoses[2] and (1→6) linkages).

β-laminarabiose and β-gentiobiose are the simplest possible models for the glycosidic linkages present in the polysaccharide schizophyllan. In this context, the increased flexibility of gentiobiose about its glycosidic linkage (compared to laminarabiose) provides support to the assumption that the lateral residues in schizopyllan show a significant degree of flexibility. Work is currently in progress to investigate directly the conformational properties of this polysaccharide by explicit-solvent molecular-dynamics simulations.[36]

Acknowledgment. Gratitude is expressed to Fabien Tran for his help in conducting the ab initio calculations. We also would like to thank the Swiss National Research foundation for the financial support received, Grants 21-63408 and 20-043568.95/1.

References and Notes

(1) Woods, R. J. *Curr. Opin. Struct. Biol.* **1995**, *5*, 591−8.
(2) Damm, W.; Frontera, A.; Tirado-Rives, J.; Jorgensen, W. *J. Comput. Chem.* **1997**, *18*, 1955−70.
(3) Kony, D.; Damm, W.; Stoll, S.; van Gunsteren, W. F. *J. Comput. Chem.* **2002**, *23*, 1416−1429.
(4) Van der Valk, P.; Marchant, R.; Wessels, J. G. H *Exp. Mycol.* **1977**, *1*, 69−82.
(5) Kuttel, M.; Brady, J. W.; Naidoo, K. J. *J. Comput. Chem.* **2002**, *23*, 1236−43.
(6) Kirschner, K. N.; Woods, R. J. *Proc. Natl. Acad. Sci.* **2001**, *98*, 10541−10545.
(7) (a) Kraus, J.; Blaschek, W.; Schuetz, M.; Franz, G. *Planta Med*. **1992**, *58*, 39−42. (b) Bohn, J. A.; BeMiller, J. N. *Carbohydr. Polym.* **1995**, *28*, 3−14. (c) Kiho, T.; Sakushima, M.; Wang, S.; Nagai, K.; Ukai, S. *Chem. Pharm. Bull.* **1991**, *39*, 798−800. (d) Kitamura, S.; Hori, T.; Kurita, K.; Takeo, K.; Hara, C.; Itoh, W.; Tabata, K.; Elgsaeter, A.; Stokke, B. T. *Carbohydr. Res.* **1994**, *263*, 111−21. (e) Kulicke, W.-M.; Lettau, A. I.; Thielking, H. *Carbohydr. Res.* **1997**, *297*, 135−143.
(8) French, A. D.; Kelterer, A.-M.; Johnson, G. P.; Dowd, M. K.; Cramer, C. J. *J. Mol. Graphics Mod.* **2000**, *18*, 95−107.
(9) Experimental values of ϕ and ψ can be found in the Cambridge Structural Database which is available at the Cambridge Crystallographic Data Centre: http://www.ccdc.cam.ac.uk/prods/csd.html.
(10) Roën, A.; Padrón J. I.; Vázquez, J. T. *J. Org. Chem.* **2003**, *68*, 4615−4630.
(11) Jeffrey, G. A.; Saenger, W. *Hydrogen bonding in biological structures*; Springer: Berlin, 1991.
(12) Casu, B.; Reggiani, M.; Gallo, G. G.; Vigevani, A. *Tetrahedron* **1966**, *22*, 3061−83.
(13) Gagnaire, D. Y.; Nardin, R.; Taravel, F. R.; Vignon, M. R. *Nouv. J. Chim*. **1977**, *1*, 423−30.
(14) Morat, C.; Taravel, F. R. *Tetrahedron Lett*. **1988**, *29*, 199−200.
(15) Tvaroska, I.; Hricovini, M.; Petrakova, E. *Carbohydr. Res*. **1989**, *189*, 359−62.
(16) Rundlöf, T.; Kjellberg, A.; Damberg, C.; Nishida, T.; Widmalm, G. *Magn. Reson. Chem.* **1998**, *36*, 839−847.
(17) Takeda, H.; Yasuoka, N.; Kasai, N. *Carbohydr. Res.* **1977**, *53*, 137−52.
(18) Dowd, M. K.; Reilly, P. J.; French, A. D. *Biopolymers* **1994**, *34*, 625−38.
(19) Rao, V. S. R.; Qasba, P. K.; Balaji, P. V.; Chandrasekaran, R. *Conformation of carbohydrates*; Harwood Academic Publishers: Chichester, U.K., 1998.
(20) Rohrer, D. C.; Sarko, A.; Bluhm, T. L.; Lee, Y. N. *Acta Cryst*. **1980**, *B36*, 650.
(21) Poppe, L. *J. Am. Chem. Soc*. **1993**, *115*, 8421−6.
(22) Ohrui, H.; Nishida, Y.; Watanabe, M.; Hori, H.; Meguro, H. *Tetrahedron Lett*. **1985**, *26*, 3251−4.
(23) (a) Rossi, C.; Ulgiati, S.; Marchettini, N. *J. Chem. Soc., Faraday Trans. 1* **1989**, *85*, 2149−58. (b) Marchettini, N.; Ulgiati, S.; Rossi, C. *Magn. Reson. Chem*. **1989**, *27*, 223−6.
(24) Poppe, L.; van Halbeek, H. *J. Magn. Reson.* **1992**, *96*, 185−190.
(25) Jorgensen, W. L.; Chandrasekhar, J.; Madura, J.; Impey, R. W.; Klein, M. L. *J. Chem. Phys.* **1983**, *79*, 926.
(26) Deslandes, Y.; Marchessault, R. H.; Sarko, A. *Macromolecules* **1980**, *13*, 1466−71.
(27) Ryckaert, J. P.; Ciccotti G.; Berendsen, H. J. C. *Mol. Phys*. **1977**, *23*, 327−41.
(28) Berendsen, H. J. C.; Postma, J. P. M.; van Gunsteren, W. F.; DiNola A.; Haak, J. R. *J. Chem. Phys.* **1984**, *81*, 3684.
(29) Haasnoot, C. A. G.; De Leeuw, F. A. A. M.; Altona, C. *Tetrahedron* **1980**, *36*, 2783−92.
(30) Imai, K.; Osawa, E. *Magn. Reson. Chem*. **1990**, *28*, 668−74.
(31) Stenutz, R.; Carmichael, I.; Widmalm, G.; Serianni, A. S. *J. Org. Chem.* **2002**, *67*, 949−958.
(32) Tvaroska, I.; Gajdos, J. *Carbohydr. Res*. **1995**, *271*, 151−62.
(33) Spoormaker, T.; De Bie, M. J. A. *Recl. Trav. Chim. Pays-Bas* **1978**, *97*, 85−7.
(34) (a) Behrends, R.; Cowman, M. C.; Eggers, F.; Eyring, E. M.; Kaatze, U.; Majewski, J.; Petrucci, S.; Richmann, K.-H.; Riech, M *J. Am. Chem. Soc.* **1997**, *119*, 2182. (b) Stenger, J.; Cowman, M. C.; Eggers, F.; Eyring, E. M.; Kaatze, U.; Petrucci, S. *J. Phys. Chem. B* **2000**, *104*, 4782.
(35) Striegel, A. M. *J. Am. Chem. Soc*. **2003**, *125*, 4146−48.
(36) Kony, D. Ph.D. Thesis, number 3421, University of Geneva, 2003.